RSC Advances

ROYAL SOCIETY OF CHEMISTRY

www.rsc.org/advances

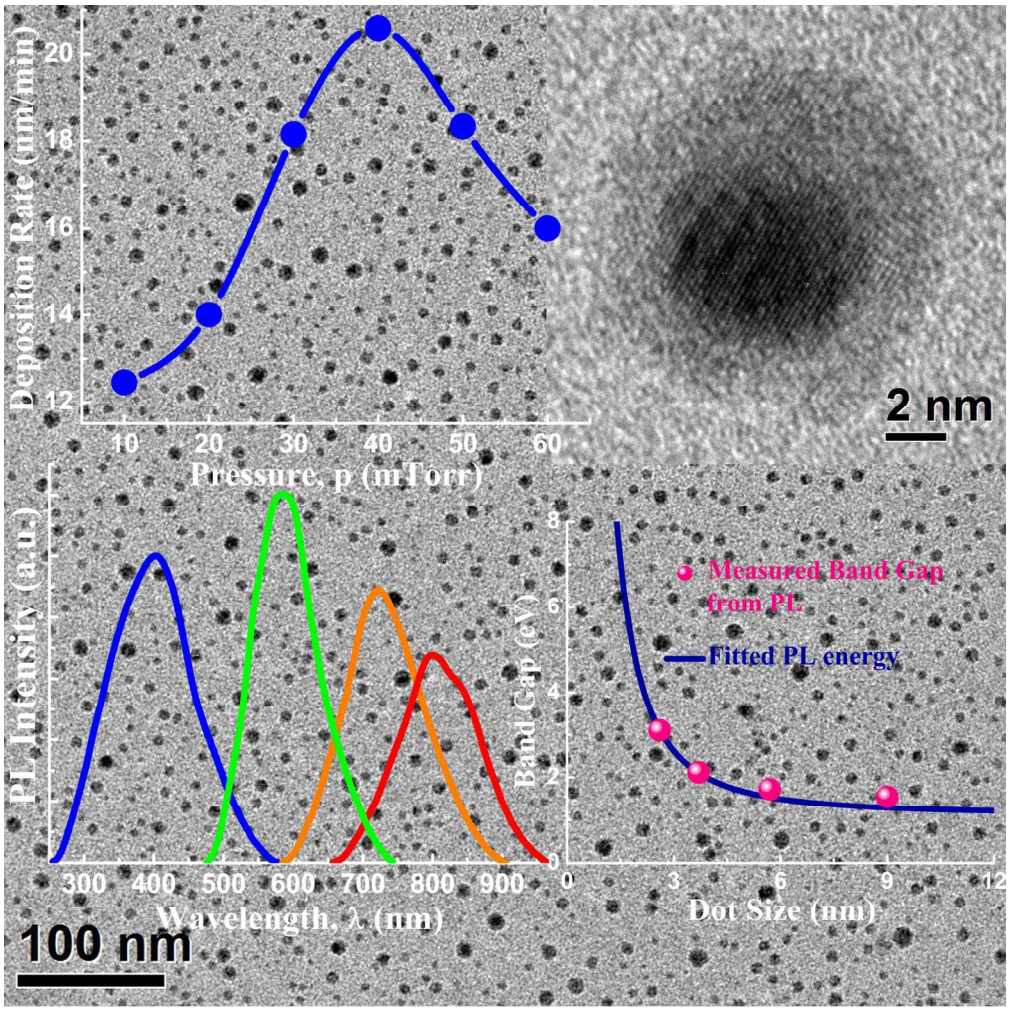

152x152mm (300 x 300 DPI)

Journal Name

ARTICLE

Rapid synthesis of nc-Si QDs thin film by plasma processing for its cost effective applications in photonic and photovoltaic devices

Received 00th January 20xx,
Accepted 00th January 20xx

DOI: 10.1039/x0xx00000x

www.rsc.org/

Debajyoti Das* and Basudeb Sain

Rapid and single step synthesis of nc-Si/a-SiN_x:H thin films with nc-Si QDs of size ~9 – 2.6 nm and number density ~10^{11}–10^{12} cm^{-2}, embedded in a-SiN_x:H matrix has been made possible from (SiH_4+ NH_3) gas mixture, with the advent of high density low pressure planar inductively coupled plasma processing. The nc-Si/a-SiN_x:H QDs films of high crystallinity ~ 80% with preferred orientation $I_{<220>}/I_{<111>}$ ~1, along with distinct presence of α-Si_3N_4 and β-Si_3N_4 components have been obtained at a competitive deposition rate of ~20.6 nm/min from an extremely low flow rate ~2.0 sccm of the feed gas SiH_4. The significance of the result lies in attaining such a material from pure SiH_4 plasma, without H_2-dilution and that even at a low substrate temperature ~ 250 °C, compatible for device fabrication. Tunable and intense visible photoluminescence (PL) with a variety of individual colors in the range 1.55–3.10 eV have been demonstrated as a consequence of band-to-band recombination due to quantum confinement effects (QCE). A high magnitude of confinement parameter ~13.5 eV nm^2 has been correlated to the core/shell-like structure of the QDs within a dielectric matrix, the amorphous shell-like component surrounding the rigid network of nc-Si QD core has been revealed by the HR-TEM micrograph. With all its various properties e.g., high crystallinity, favored orientation, wide optical gap due to the quantum confinement in Si-ncs and significant amount of nitrogen bonding in the matrix as well as tunable wide range photoluminescence, the nc-Si/a-SiN_x:H quantum dots (QDs) thin films deserve enormous promise for cost effective application in silicon based photonic and photovoltaic devices.

1. Introduction

Since long silicon is the backbone of the semiconductor industry for its versatile and environment friendly properties. However, silicon technology does not allow an easy integration of electronics with the photonic components since silicon is a poor light emitter due to its indirect band gap. The discovery of light emission in nanostructured silicon in the 1990s opened up new avenues of research in nano-silicon based devices.[1,2] One such pathway is the application of silicon quantum dots in advanced photovoltaic[3] and light emitting devices.[4-6] Nanocrystalline silicon (nc-Si) films are mixed-phase materials containing a crystalline Si phase embedded within an amorphous matrix. The nc-Si film possesses superior properties than its amorphous counterparts e.g., high stability against light soaking, high doping efficiency, improved absorption properties and can emit light of different wave lengths with the help of band gap engineering by miniaturization of the size of Si-nanocrystals.[7-9] The low absorption and emission in bulk silicon are due to the participation of a phonon to conserve both energy and momentum. This three-particle interaction (electron, hole and phonon) makes the process less probable.[10] As the mechanism of phonon mediated light emission is the inverse of the photoelectric effect, the absorption properties depend strongly on the emission. Nanocrystalline silicon-nitride (nc-Si/a-SiN_x:H) thin films in which silicon-nanocrystals (Si-nc) that exhibit quantum size effect are embedded in a-SiN_x:H dielectric matrix have attracted considerable research interest due to its potential applications in solar cells, thin film transistors and light-emitting devices.[11-15] Silicon-nitride (SiN_x) is being introduced as a material of high dielectric constant, high strength over a wide temperature range, low tunneling barrier as well as outstanding chemical inertness. Besides these, it has excellent inherent antireflection and surface passivation properties which are very important for enhancement of device performance.[16-17]

In general, the formation of nc-Si QDs is being pursued through conventional capacitively coupled radio frequency plasma enhanced chemical vapour deposition (rf-PECVD) that requires a high hydrogen dilution, high rf power density and temperature, owing to the need to enhance atomic hydrogen density and available thermal energy which help nano-crystallization. High hydrogen dilution results in a low growth rate (typically, a few nm/min) that severely retards the cost-effective production of nc-Si QDs based devices which happens to be unfavorable from commercial point of view. High rf power causes surface damage by high-energy ion bombardment that reduces the device performance and high deposition temperature reduces the device feasibility on inexpensive soft substrates. In comparison, inductively coupled plasma (ICP) operating in the electromagnetic mode has several major qualities e.g., it possess i) high densities of the plasma species, ii) low plasma sheath potentials near the chamber wall or substrate, which is beneficial for the reduction of ion bombardment on the deposited films, iii) low electron temperatures in a broad range of discharge conditions and iv) excellent uniformity of the plasma parameters in the radial and axial directions. Inductively coupled plasma (ICP), produces high-density plasma at low pressure that facilitate

Nano-Science Group, Energy Research Unit,
Indian Association for the Cultivation of Science,
Jadavpur, Kolkata – 700 032, INDIA
** E-mail (D. Das): erdd@iacs.res.in; Fax: +91(33)24732805*

crystallization even at low temperature and simultaneously maintains a superior deposition rate without any surface damage.[18-19]

Present report deals with the single step development of the thin film of nc-Si QDs embedded in the a-SiN_x:H dielectric matrix, through spontaneous rf inductively coupled plasma processing at significantly low pressure in the mili-Torr range. The nc-Si-QDs/ a-SiN_x:H thin films of very high crystallinity and favored crystalline orientation, demonstrating tunable wide range (1.55–3.10 eV) visible photoluminescence are grown at low temperature with high deposition rates using very low flow rate of SiH_4 and NH_3, without H_2-dilution. Various characterizations have been performed in order to establish a correlation among the structural, morphological, compositional and optical properties of the films for their applications in photonic, optoelectronic and photovoltaic devices.

2. Experimental Details

2.1 Materials Development

Inductively Coupled radio frequency (13.56 MHz) low-pressure plasma was employed to prepare silicon-nitride films on p-type (100) silicon substrates, Corning® Eagle2000™ glass and carbon coated copper microscope grids. A mixture of silane (SiH_4) and ammonia (NH_3) were used as reactant gas sources, maintaining a flow rate ratio SiH_4 : NH_3 = 2 sccm : 0.3 sccm. The growth temperature and plasma power during deposition were fixed at 250 °C and 375 W, respectively, while the chamber pressure was varied from 10 to 60 mTorr. No post-deposition annealing process was employed after growing the silicon nitride films.

2.2 Characterizations of the Materials

Thickness of the films was determined by a Dektak 6M stylus profiler. For uniform comparison, thickness of all the films was maintained at ~4000 Å. The Raman spectra were obtained by Renishaw inVia Micro-Raman spectrophotometer (Serial No. 12W143) at room temperature in a backscattering geometry, using 514 nm Ar^+ Laser as the excitation source, at a power density of 2 mW/cm^2. The X-ray diffraction analysis was carried out using a conventional Cu K_α X-ray radiation (λ=1:5418 Å) source and a Bragg diffraction set-up (Seifert 3000P). High-resolution transmission electron micrographs (HR-TEM) were obtained on ~30 nm thick samples deposited on carbon coated copper microscope grids supplied by Pacific Grid-Tech, USA, using a JEOL-JSM2010 transmission electron microscope operating at 200 kV. The X-ray photoelectron spectroscopy (XPS) of the films was performed using a focused monochromatized Al-Kα X-ray source (1486.8 eV) in the XPS instrument (Omicron Nano Technology 0571). The room temperature PL spectra were obtained using a He-Cd laser source, with a uniform excitation of 325 nm. The luminescence spectrum was monitored using a TRIAX 320 monochromator fitted with a cooled Hamamatsu R928 photomultiplier detector.

3. Results and discussion

3.1 Deposition Rate

Fig. 1 shows the variation of the deposition rate, R_d, of the nc-Si/ a-SiN_x:H thin films as a function of gas pressure, p, in the plasma. At the lowest pressure, p= 10 mTorr the film grows with R_d ~12.5 nm/min. On increase in the gas pressure, R_d has been found to increase very rapidly attaining the maximum magnitude, $(R_d)_{max}$ ~20.6 nm/min at an optimum pressure, p= 40 mTorr beyond which R_d reduces on further increase in p. A deposition rate of ~20.6 nm/min appears to be very competitive, considering the growth of nc-Si/a-SiN_x:H film using very low flow rate (2.0 sccm) of the feedstock SiH_4 which has been in effect by virtue of efficient dissociation of gas molecules by high density inductively coupled plasma even at a moderate power of 375 W.[20-22] Cheng et al. previously reported a very high growth rate (2.37 nm/s) in the development of nc-Si films, using similar rf inductively coupled plasma; however, in that case a very high flow rate of SiH_4 (36 sccm) and high rf power (2000 W) was used.[23]

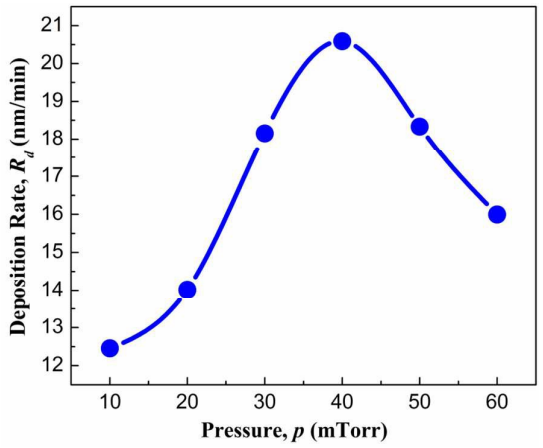

Fig. 1 Variation of the deposition rate, R_d as a function of deposition pressure, p.

3.2 Raman studies

Fig. 2 presents the Raman spectra of the samples deposited at different pressure, p. The dominant Raman peak at around 430 to 550 cm^{-1} is asymmetric in shape with an extended tail towards lower wave numbers and is attributed to the transverse optical (TO) mode of Si–Si vibrations.[24] A significant change in the line shape along with a continuous up-shift of peak frequency, as presented by the magnified view of the peaks at the inset in Fig. 2, has been identified during increase in p from 10 to 40 mTorr, attributing

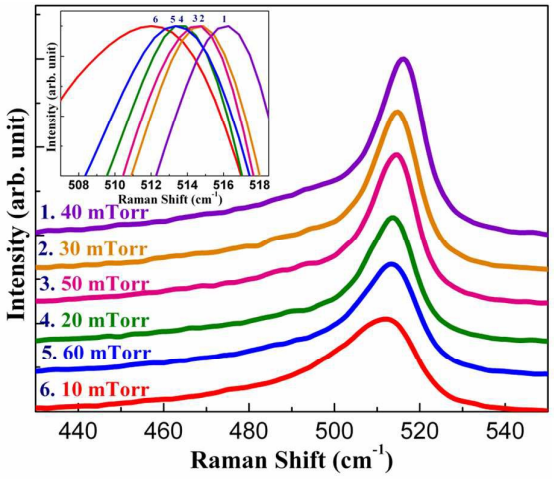

Fig. 2 First order Raman spectra at different p. Inset presents the magnified view of the peaks of the Raman spectra.

modification in the nature of the network structure with simultaneous change in the size of silicon nanocrystallites. For a further increase of pressure, however, the peak red shifts. The quantitative estimation of the crystalline volume fraction in each sample has been performed by the deconvolution of each Raman spectrum into three Gaussian sections at ~515, ~480 and <510 cm^{-1} corresponding to nanocrystalline (nc-Si), amorphous (a-Si) and the intermediate ultra-nanocrystalline (unc-Si) component, respectively. The volume fractions of the individual components are estimated and the total crystalline volume fraction (X_C) is obtained as: $X_C = X_{nc} + X_{unc}$.[25] The overall crystallinity increases, from ~59 to 80%, with increasing deposition pressure from 10 to 40 mTorr beyond which the network crystallinity decreases and attains a magnitude ~63% at p = 60 mTorr. On the contrary, the ultra-nanocrystalline fraction, X_{unc}, decreases monotonically from ~36 to 22% with increase of pressure over the entire span, from 10 to 60 mTorr, as shown in Fig. 3a.

The average grain size has been estimated from Raman spectrum using the relation[25]

$$\left[\omega_L - \omega_0\right]^2 + \left(\frac{\Gamma_0}{2}\right)^2 \cong \frac{1}{3L} \cdot exp\left(-\pi^2\right) \qquad (1)$$

where ω_L is the frequency of the crystalline-like mode, for nanocrystals of size L. The ω_0 and Γ_0 are 520 and 3.5 cm^{-1}, respectively, for crystalline silicon. In our previous works[25-26] a comparison between the estimated size from XRD, HR-TEM and Raman data using Eq. 1 was reported and a close proximity in grain sizes estimated from above mentioned three different processes was observed that established the general acceptance of Eq. 1 for finding out the grain size from Raman spectra. The size of nc-Si QDs, estimated from the deconvoluted line-shape of the nanocrystalline components, demonstrates a Gaussian-like distribution with its maximum magnitude ~9 nm at p = 40 mTorr to a minimum of ~3±0.5 nm at both reduced and enhanced pressure, as shown in Fig. 3b.

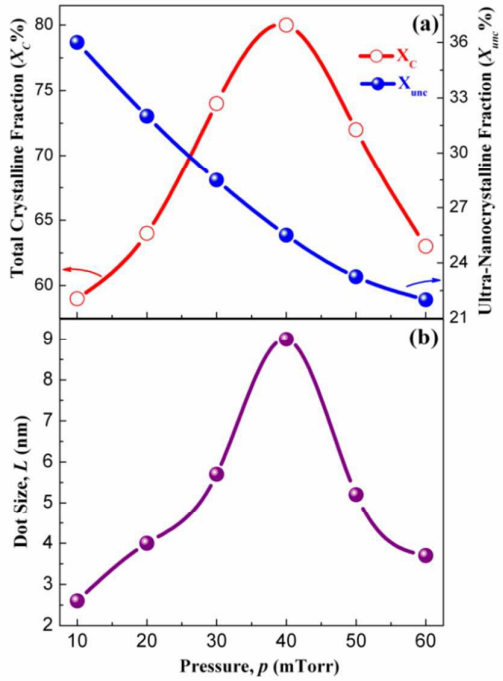

Fig. 3 (a) Variations of the total crystalline volume fraction (X_C) and ultra-nanocrystalline volume fraction (X_{unc}) with deposition pressure, p. (b) Variations of the size of nc-Si QDs estimated from the shift of the first order Raman spectra with p. Largest size of QDs are related to the highest crystalline volume fraction corresponding to p= 40 mTorr.

3.3 X-ray diffraction studies

Fig. 4 represents the X-ray diffraction (XRD) spectra for the films prepared at different pressure, p. The broad band centered at 2Θ ~25° corresponds to the amorphous silicon component. However, the peaks at 2Θ = 28.34°, 47.17° and 56.08° correspond to (111), (220) and (311) crystallographic planes of silicon, respectively. The diffraction intensities of each peak increase monotonically with increasing pressure up to 40 mTorr beyond which it decreases gradually, suggesting a Gaussian-like distribution of crystallinity in the silicon network over the span of pressure studied. The XRD peaks corresponding to <111> orientation are, in general, most intense, i.e., the silicon crystallites are preferentially grown along <111> crystallographic orientation. However, the relative intensity of the <220> peak, $I_{(220)}/I_{(111)}$, gradually increases and attains ~1, i.e., the <220> peak becomes of an equal strength to that of <111> peak on increase in p at 40 mTorr, as shown in the inset of Fig. 4. On further increase of p, $I_{(220)}/I_{(111)}$ reduces and attains a virtual saturation. The <111> orientation arises from random nucleation whereas, <220> due to the growth of thermodynamically preferred grains.[24,27] The nature of variation of $I_{(220)}/I_{(111)}$ indicates the preferential formation of a large fraction of thermodynamically preferred crystalline grains in the nitrogenated silicon network on increasing pressure up to an optimum magnitude and that corresponds to the gradually increasing overall crystallinity (X_C), estimated from Raman studies (Fig. 3a).

Besides the crystallites of silicon, the network also contains tiny crystallites of silicon-nitride (Si_3N_4), the signature of which has been identified by the corresponding (301) crystallographic plane of α-Si_3N_4 at around 2Θ = 43.40° and β-Si_3N_4 at around 2Θ = 41°.[9,28,29]

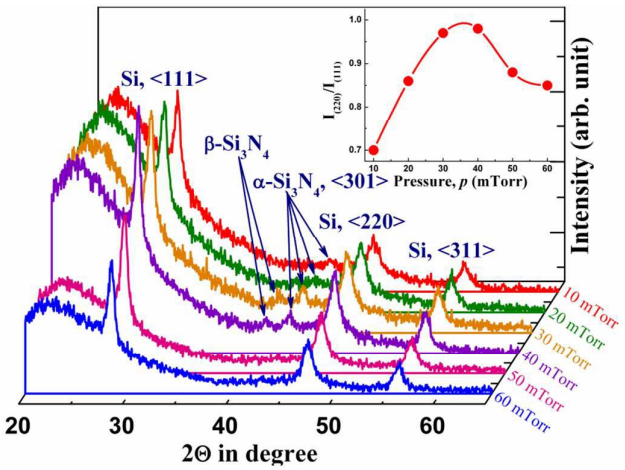

Fig. 4 X-ray diffraction spectra of nc-Si/a-SiN_x:H QDs thin films prepared at different pressure, p, varying from 10 to 60 mTorr. Inset shows the variation of $I_{(220)}$ /$I_{(111)}$, with p. Most intense α-Si_3N_4 and β-Si_3N_4 component peaks in the XRD spectra accompany with the highest $I_{(220)}/I_{(111)}$ of ~1, corresponding to samples prepared at p= 30 and 40 mTorr.

The maximum peak intensity of the α-Si_3N_4 and β-Si_3N_4 component peaks in the XRD spectra are detected for samples prepared at p= 30 and 40 mTorr where $I_{(220)}/I_{(111)}$ of the nc-Si peaks attaine the maximum magnitude of ~1 and the overall crystallinity are very high as well as the grain sizes are relatively large. With further higher pressure at p = 50 and 60 mTorr the Si_3N_4 components virtually disappear. The Si grains with <220> crystallographic orientation remains conducive to the electrical transport in stacked layer devices.[30] In particular, best values of open-circuit voltage (V_{OC}) in solar cells identifies low recombination losses in <220> textures.[31] Accordingly, the nc-Si/a-SiN_x:H thin films prepared at p in the range 30–40 mTorr appears highly appropriate for utilization in the fabrication of tandem structure Si solar cells.

3.4 Transmission electrom microscopy

Details of the internal microstructure are obtained from the high-resolution transmission electron microscopy (HRTEM). Because of our interest in nc-Si structures within quantum dot configuration, i.e., with size ≤ Bohr radius of silicon, the plain-view bright field micrographs of the samples prepared at p = 30 and 10 mTorr have been displayed in Fig. 5a and 5c, respectively, wherein the Si-QDs are identified as denser material with relatively dark appearance, randomly distributed within a less dense matrix.[26,32,33] The magnified view of the microstructure of an arbitrarily chosen single QD for each sample has been presented in Fig. 5b and 5d, respectively. Well identified crystal planes are noticeable in the marked circular area, demonstrating spherical-like shape of the nc-Si–QDs. The fast Fourier transform (FFT) pattern of the corresponding high magnification images identify a <220> orientation in Fig. 5b and a <111> orientation in Fig. 5d. Because of the specific geometrical projection on two-dimensional plane, the <220> crystal planes are relatively difficult to be visible in plain-view HR-TEM micrograph, compared to its <111> counterpart. An effortless detection of the (220) lattice planes within the Si QDs establish the presence of significant number of <220> oriented Si nanocrystallites within the hydrogenated amorphous silicon-nitride (a-SiN_x:H) matrix prepared at p = 30 mTorr, where significantly high magnitude of $I_{(220)}/I_{(111)}$ ~ 1 has been demonstrated by the XRD studies. In case of p = 30 mTorr, the nc-Si–QDs are mostly of <111> crystallographic orientation.

Careful observation reveals that both the individual nc-Si QDs are surrounded by a layer of finite thickness which is dark and dense relative to the surrounding amorphous matrix, but do not possess any lattice plane. Comparing with our previous studies on nc-Si QDs within silicon-oxide matrix, this adjoining layer may be estimated as shell covering the nc-Si QDs core isolating those from the amorphous silicon-nitride matrix in which those are embedded.[34] The amorphous shells act as protective layers for confining the nanocrystalline core and play crucial roles in controlling their size and number density. A Gaussian like distribution of nc-Si QDs in each sample is presented by the corresponding histograms in Fig. 5a and 5c. The average size and number density of the nanocrystals have been identified from the corresponding peak of the distributions. A relatively sharp size distribution with FWHM ~0.9 nm, corresponding to the average size ~5.86 nm and number density ~1.16×10^{12} cm^{-2} are obtained in samples prepared at p = 30 mTorr; while tiny nc-Si QDs of average size ~2.72 nm, with a higher density~3.8×10^{12} cm^{-2} and wider size distribution (FWHM~1.18 nm) are obtained at p =10 mTorr. It is interesting to note that the HRTEM estimated average sizes, 5.86 and 2.72 nm for samples prepared at p = 30 and 10 mTorr, respectively, are in close proximity with the same, 5.7 and 2.6 nm, respectively, obtained from Raman analysis using Eq. 1.

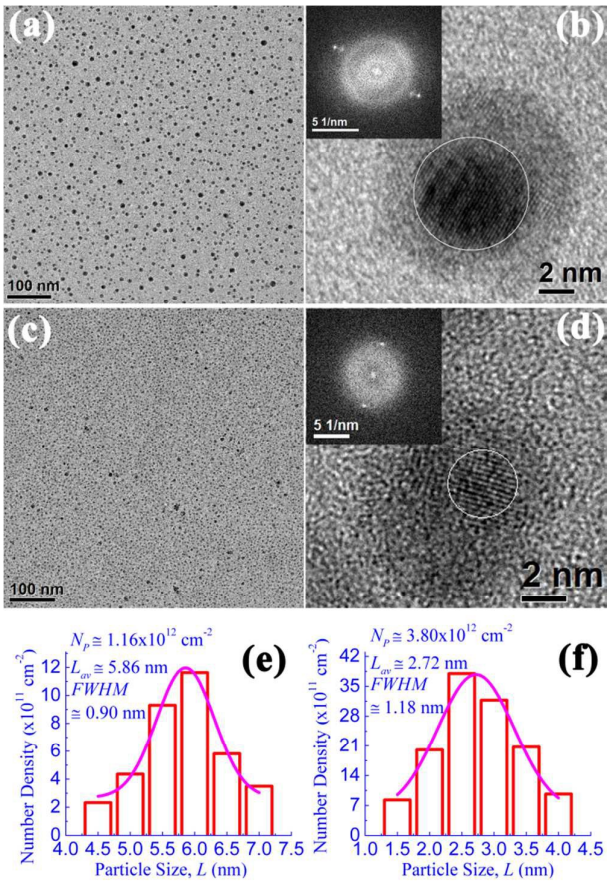

Fig. 5 (a), (b) and (c), (d) are the HR-TEM micrographs with low and high magnifications for the nc-Si/a-SiN_x:H QDs films prepared at p = 30 and 10 mTorr, respectively; corresponding histograms in (e) and (f) demonstrate the distribution of number density with size of the Si nanocrystals. The FFT patterns at the insets in (b) and (d) demonstrate the corresponding orientations of the crystalline planes of nc-Si QDs which are <220> and <111>, respectively.

3.5 Studies by XPS

Fig. 6 presents a typical survey scan XPS spectrum of the sample prepared at p = 10 mTorr. The predominant peaks occurring in the spectrum are from Si and N elements accompanied by several minor peaks attributed to C and O elements. The C and O peaks may arise from the residual surface contamination at the inner wall of the vacuum chamber or the post deposition adsorbents on the sample surface. The nitrogen concentration has been estimated from the narrow scan XPS spectra of N 1s with corresponding peak centered at 398.8 eV as presented in the inset of Fig. 6, and that significantly reduces from ~35 at.% for sample prepared at p = 10 mTorr to ~15 at.% at p = 30 mTorr.[35,36]

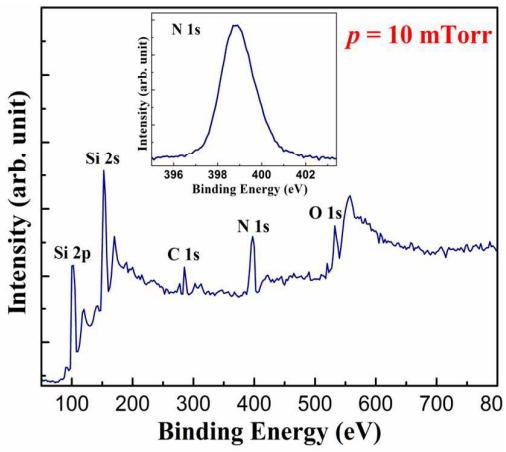

Fig. 6 A typical survey scan XPS spectrum of the sample at p = 10 mTorr. Inset shows the narrow scan XPS spectrum for N 1s.

3.6 Photoluminescence studies

The photoluminescence (PL) spectra of a variety of individual colors in the visible range have been demonstrated by the nc-Si/a-SiN_x:H quantum dots (QDs) thin films under 325 nm excitation by He-Cd laser, as shown in Fig. 7. With the variation of pressure from 10 to 40 mTorr the PL peak shifts from near UV at ~ 400 nm (3.1 eV) to near IR at ~800 nm (1.55 eV) region. Relatively wide size distribution and higher number density of the nc-Si QDs in sample prepared at p = 10 mTorr, as observed from the corresponding histograms attached with TEM micrograph in Fig. 5, may be accounted for its broader PL band and enhanced PL intensity, respectively, compared to the sample prepared at p = 30 mTorr.

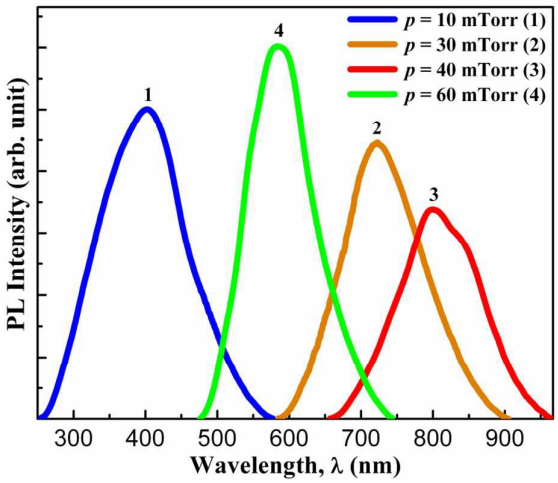

Fig. 7 Room temperature photoluminescence (PL) spectra, under 325 nm excitation by He-Cd laser, of nc-Si/a-SiN_x:H QDs thin films deposited by ICP-CVD at different pressures, p.

The shifts of the PL and Raman bands pursuing in opposite directions raise the possibility of quantum confinement effect as the origin of photoluminescence.[37-40] According to the effective mass theory, the energy gap, E, for three-dimensionally confined silicon nanocrystals can be expressed as:[32,41]

$$E = E_{bulk} + Q / L^2 \qquad (2)$$

where E_{bulk} is the bulk crystal silicon band gap, L the dot size, and Q the confinement parameter. The variation in the band gap energy (E, in eV) of the nc-Si/a-SiN_x:H QDs thin films, estimated from the associated PL peak position, has been plotted in Fig. 8, as a function of average size (L, in nm) of the QDs. Considering the quantum confinement phenomena occurring in the silicon–nitrogen–hydrogen complex system, the least square fit plot to the data in the form of above equation leads to the semi-empirical relation:

$$E = 1.10 + 13.5 / L^2 \qquad (3)$$

where E_{bulk} = 1.10 eV matches well with the literature and very high quantum confinement parameter, Q = 13.5 eV nm^2 have been demonstrated.

Previously, Q =13.9 eV nm^2 was reported for Si-QDs embedded in SiN_x matrix grown from capacitively coupled (SiH_4 + NH_3)-plasma,[42] while Q = 11.8 eV nm^2 was obtained using (SiH_4 + N_2)-plasma.[43] Confinement parameters of relatively much lower

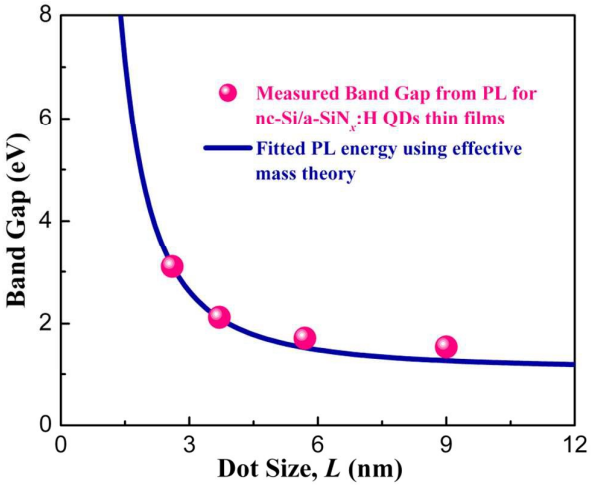

Fig. 8 Band gap widening on reduction in the size of nc-Si QDs. Data: (pink circle) obtained from PL peak position and (navy line) fitted PL data using effective mass theory. Reasonably good match between data and the plot demonstrates quantum confinement phenomena to occur in the silicon-nitrogen-hydrogen heterostructure.

magnitude, e.g., 2.4 eV nm^2 were reported in the case of a-Si QDs in a SiN_x matrix.[44,45] We have reported earlier, Q = 11.6 eV nm^2 for nc-Si QDs embedded in a-Si/SiO_x matrix, obtained from He-diluted (SiH_4 + CO_2)-plasma.[32] A higher magnitude of Q was identified as the signature of enhanced quantum confinement effects occurring in Si-QDs when grown from NH_3-plasma compared with N_2 plasma and was attributed to the enhancement in crystallinity as well as surface passivation of Si-QDs mostly by H derived from NH_3. The value of Q estimated from the current set of samples is comparably high (Q ~13.5 eV nm^2), which can be considered as a consequence of the core-shell like structure of the nc-Si QDs, facilitating confinement of charge carriers within the crystalline core.[32] A large amount of atomic hydrogen flux that originates due to the high degree dissociation of the gas molecules in high-density inductively coupled plasma (ICPs) helps growing plenty of ultra-nanocrystallites and passivation of the nonradiative dangling bonds and thereby, demonstrating intense visible photoluminescence.

In general, the nanocrystalline silicon thin films are commonly synthesized by using plasma processing of precursor gases highly diluted in hydrogen that results in a low growth rate (typically, a few nm/min).[21,46-48] This severely retards the cost-effective production of nc-Si based devices. Furthermore, although high hydrogen dilution indeed promotes non epitaxial nanocrysalline growth, excessive hydrogenation leads to poor material performance (e.g., degradation upon light exposure, etc.) in solar cells and other devices. On the contrary, the present work considers deposition of nc-Si/a-SiN_x:H QDs thin films with even 80% crystallinity and at very high growth rate, R_d ~20.6 nm/min, using inductively coupled plasma processing without H_2 dilution, at a low temperature.

In the present deposition system the plasma is generated by a built in four-antenna low inductance flat spiral coil and the plasma is confined at the vicinity of the quartz plate of ICP source. ICP-discharges are produced by the rf power applied across a dielectric window via electromagnetic coupling that happens to be advantageous for generating higher plasma density, lower plasma sheath potentials at the growth surface etc., compared to different other low-pressure plasma discharges. The substrate holder is located at a distance so as to keep the growth zone away from direct plasma exposure. Accordingly, the gas-phase transport of the precursors onto the substrate surface can be easily controlled by adjusting the gas pressure. The overall chemistry is initiated by fast gas phase reactions of small radicals, e.g. SiH_3 and NH_2. Mass spectrometric studies reveal that aminosilanes, $SiH_x(NH_2)_{4-x}$ (x = 0 − 3), are directly formed in the gas phase and aminosilylenes, $HSiNH_2$, are formed as a reactive intermediate. In addition, higher silane (disilane/trisilane) may also be produced in the plasma in parallel.[49] Different heterogeneous reactions of these precursors are considered to be the viable pathway for film growth. At a low pressure of 10 mTorr, low deposition rate ~12.5 nm/min is a consequence of low number densities of SiH_3 and NH_2 radicals available in the plasma. At an elevated gas pressure, although the number density of radicals and ions increases in the plasma, their reactivity on the growing surface is reduced because of reduced mean free path due to multiple inter-collisions before arrival at the growth site. However, the less reactive silyl (SiH_3) and the aminosilylene ($HSiNH_2$), those are formed at gas phase, can favorably diffuse onto the growing surface and develop the ordered network of silicon crystallites in silicon-nitride with higher deposition rate.[49] Atomic hydrogen generates in the plasma through the simultaneous dissociation of SiH_4 and NH_3 gas molecules. With increase of pressure, the atomic hydrogen density increases that help to produce larger size grains with lower density.[50] It is evident from the Raman spectra (Fig. 3) that the crystallinity increases with increased grain size up to the chamber pressure of 40 mTorr. In the present work, the overall crystallinity of the samples is estimated to be significantly high, varying within ~80 to 59 %. The overall high crystallinity at rapid deposition is the unique feature of high-density inductively coupled plasma. The high surface coverage by atomic hydrogen from high degree dissociation of gas molecules increases surface diffusion length of the radicals. The large surface diffusion length facilitates the adsorbed radicals in reaching the energetically convenient positions on the growing surface and produces higher crystalline films.[51,52] Larger surface diffusion length at higher pressure is responsible for having higher amount of crystallinity in the films. A significant fraction of Si dangling bonds is partially terminated by reactive hydrogen atoms, which in turn reduces the Gibbs free energy (G) and the lower G is particularly favorable for the nucleation of Si QDs and that enables the formation of controlled nanocrystalline silicon-nitride film in nc-Si/a-SiN_x:H QDs configuration.[53,54] An enhancement in average QDs size from 2.72 to 5.86 nm and the corresponding decrease in the number density from ~3.8×10^{12} to 1.16×10^{12} cm^{-1} with simultaneous broadening in the particle distribution are observed from HRTEM micrographs in Fig. 5, as pressure increases from 10 to 30 mTorr.

The present work signifies the rapid single step development of self-assembled nc-Si/a-SiN_x:H QDs thin films of varying dot size, ~9 to 2.6 nm, with high number density, ~10^{11}–10^{12} cm^{-2}, using extremely low flow rate of precursor gases (SiH_4 = 2 sccm, NH_3 = 0.3 sccm), by rf inductively coupled plasma-CVD, at very low deposition pressure (10–60 mTorr) and low growth temperature (250 °C). The nc-Si/a-SiN_x:H QDs thin films demonstrate visible photoluminescence, tunable over wide range (1.55–3.1 eV), with very high magnitude of the confinement parameter (Q ~13.5 eV nm^2) and thereby, possess enormous promise towards the fabrication of cost effective silicon based photonic, optoelectronic and photovoltaic devices.

4. Conclusions

Rapid growth and the single step development of nc-Si-QDs/ a-SiN_x:H thin films have been obtained by rf (13.56 MHz) inductively coupled low pressure plasma processing of a mixture of silane (SiH_4) and ammonia (NH_3) gases at a low growth temperature (250 °C). In the films the nanocrystalline silicon quantum dots (nc-Si QDs) of varying size ~9 to 2.6 nm, with number density ~10^{11}–10^{12} cm^{-2} are embedded in hydrogenated amorphous silicon-nitride (a-SiN_x:H) matrix.

Important results include the formation of a very high crystallinity ~ 80% with grain size ~ 9 nm having comparable strength of thermodynamically favorable <220> crystallographic orientation to that of random <111> orientation along with distinct signatures of growth of α-Si_3N_4 and β-Si_3N_4 components. The films are obtained at a competitive deposition rate of ~20.6 nm/min from an extremely low flow rate (2.0 sccm) of the feed gas SiH_4 at an optimum pressure, p= 40 mTorr. The significance of the result lies in attaining such a material from pure SiH_4 plasma, without H_2-dilution and that even at a low substrate temperature ~ 250 °C compatible for device fabrication.

Intense visible photoluminescence (PL) with a variety of individual colors in the range 1.55–3.10 eV have been exhibited by the nc-Si/a-SiN_x:H quantum dots (QDs) thin films. The shifts of the PL and Raman bands pursuing in opposite directions demonstrate band-to-band recombination due to quantum confinement effect (QCE) as the origin of photoluminescence. A high magnitude of confinement parameter ~13.5 eV nm^2 has been correlated to the core/shell-like structure of the QDs within a-SiN_x:H matrix. The amorphous shell-like component surrounding the rigid network of nc-Si QD core has been revealed by the HR-TEM micrograph.

With all its various properties e.g., high crystallinity, favored orientation, wide optical gap due to the quantum confinement in Si-ncs and significant amount of nitrogen bonding in the matrix as well as tunable wide range photoluminescence, the nc-Si/a-SiN_x:H quantum dots (QDs) thin films deserve enormous promise for cost effective application in silicon based photonic and photovoltaic devices.

Acknowledgements

The work has been done under nano-silicon projects funded by the Department of Science and Technology (Nano-Mission Program) and the Council of Scientific and Industrial Research, Government of India. The HR-TEM and XPS studies have been performed using facilities of Unit on Nano-Science at IACS. One of the authors (B.S.) acknowledges the Council of Scientific and Industrial Research, Government of India, for providing him with a research fellowship (via Grant No. 09/080(0706)/2010-EMR-I) for the work.

References

1 L. T. Canham, *Appl. Phys. Lett.*, 1990, **57**, 1046.

2 A. G. Cullis and L. T. Canham, *Nature*, 1991, **353**, 335.

3 E. C. Cho, M. A. Green, G. Conibeer, D. Song, Y. H. Cho, G. Scardera, S. Huang, S. Park, X. J. Hao, Y. Huang and L. Van Dao, *Adv. OptoElectron.*, 2007, **2007**, 69578.

4 L. Pavesi, L. Dal Negro, C. Mazzoleni, G. Franzo and F. Priolo, *Nature*, 2000, **408**, 440.

5 Z. Yuan, O. Anopchenko, N. Daldosso, R. Guider, D. Navarro-Urrios, A. Pitanti, R. Spano and L. Pavesi, *Proc. IEEE*, 2009, **97**,1250.

6 R. J. Walters, G. I. Bourianoff and H. A. Atwater, *Nat. Mater.*, 2005, **4**, 143.

7 S. Huang and S. Oda, *Appl. Phys. Lett.*, 2005, **87**,173107.

8 P. M. Fauchet, *Materials Today*, 2005, **8**, 26.

9 Y. H. So, S. Huang, G. Conibeer and M. A. Green, *EPL*, 2011, **96**, 17011.

10 L. E. Brus, P. J. Szajowski, W. L. Wilson, T. D. Harris, S. Schuppler and P. H. Citrin, *J. Am. Chem. Soc.*1995, **117**, 2915.

11 K. S. Cho, N. M. Park, T. Y. Kim, K. H. Kim, G. Y. Sung and J. H. Shin, *Appl. Phys. Lett.*, 2005, **86**, 071909.

12 A. K. Panchal, D. K. Rai, M. Mathew and C. S. Solanki, *Nano*, 2009, **04**, 265.

13 G. Y. Sung, N. M. Park, J. H. Shin, K. H. Kim, T. Y. Kim, K. S. Cho and C. Huh, *IEEE J. Quantum Electron.*, 2006, **12**, 1545.

14 G. Conibeer, M. Green, E. C. Cho, D. König, Y. H. Cho, T. Fangsuwannarak, G. Scardera, E. Pink, Y. Huang, T. Puzzer, S. Huang, D. Song, C. Flynn, S. Park, X. Hao and D. Mansfield, *Thin Solid Films*, 2008, **516**, 6748.

15 B. Sain and D. Das, *RSC Adv.*, 2014, **4**, 36929.

16 S. Duttagupta, F. Ma, B. Hoexa, T. Muellera and A. G. Aberle, *Energy Procedia*, 2012, **15**, 78.

17 Q. J. Cheng, S. Xu and K. Ostrikov, *J. Mater. Chem.*, 2010, **20**, 5853.

18 K. Ostrikov, *Rev. Mod. Phys.*, 2006, **77**, 489.

19 Q. J. Cheng, S. Xu and K. Ostrikov, *Acta Mater.*, 2010, **58**, 560.

20 S. R. Jadkar, J. V. Sali, M. G. Takwale, D. V. Musale and S. T. Kshirsagar, *Thin Solid Films*, 2001, **395**, 206.

21 S. Mukhopadhyay, C. Das and S. Ray, *J. Phys. D : Appl. Phys.*, 2004, **37**, 1736.

22 M. Scheib, B. Schröder and H. Oechsner, *J. Non-Cryst. Solids.*, 1996, **198–200**, 895.

23 Q. J. Cheng, S. Xu, S. Y. Huang and K. Ostrikov, *Cryst. Growth Des.*, 2009, **9**, 2863.

24 D. Raha and D. Das, *Solar Energy Mater. Sol. Cells*, 2011, **95**, 3181.

25 B. Sain and D. Das, *Sci. Adv. Mater.*, 2013, **5**, 188.

26 D. Das and B. Sain, *J. Appl. Phys.*, 2013, **114**, 073708.

27 V. L. Dalal, K. Muthukrishnan, X. Niu and D. Stieler, *J. Non-Cryst. Solids*, 2006, **352**, 892.

28 O. R. Monteiro, Z. Wang and I. G. Brown, *J. Mater. Sci.*, 1996, **31**, 6029.

29 S. Pasupuleti, R. Peddetti, S. Santhanam, K. P. Jen, Z. N. Wing, J. P. Halloran and M. Hecht, *J. Mater. Sci.*, 2008, **43**, 2799.

30 J. H. Werner, K. Taretto, U. Rau, *Solid State Phenom.*, 2001, **80**, 299.

31 E. Vallat-Sauvain, A. Shah and J. Bailat, *Advances in Microcrystalline Silicon Solar Cell Technologies in Thin Film Solar Cells: Fabrication, Characterization, and Application*, in: J. Poortmans, V. Arkhipov (Eds.). first ed. England: John Wiley and Sons; 2007, pp. 13–171.

32 D. Das and A. Samanta, *Nanotechnology*, 2011, **22**, 055601.

33 M. Jana, D. Das and A. K. Barua, Sol. Energy Mater. Sol. Cells, 2002, **74**, 407.

34 D. Das and A. Samanta, *Mater. Res. Bull.*, 2012, **47**, 3625.

35 Z. Q. Yao, P. Yang, N. Huang, H. Sun, G. J. Wan, Y. X. Leng, J. Wang and J. Y. Chen, *Surf. Coat. Technol.*, 2006, **200**, 4144.

36 J. Szépvölgyi, I. Mohai and J. Gubicza, *J. Mater. Chem.*, 2001, **11**, 859.

37 B. Sain and D. Das, *Phys. Chem. Chem. Phys.*, 2013, **15**, 3881.

38 D. Das, *Solid State Commun.*, 1998, **108**, 983.

39 B. Sain and D. Das, *J. Lumin.*, 2015, **158**, 11.

40 D. Das, *Thin Solid Films*, 2005, **476**, 237.

41 L. W. Wang and A. Zunger, *J. Phys. Chem.*, 1994, **98**, 2158–2165.

42 T. W. Kim, C. H. Cho, B. H. Kim and S. J. Park, *Appl. Phys. Lett.*, 2006, **88**, 123102.

43 T. Y. Kim, N. M. Park, K. H. Kim, G. Y. Sung, Y. W. Ok, T. Y. Seong and C. J. Choi, *Appl. Phys. Lett.*, 2004, **85**, 5355.

44 N. M. Park, C. J. Choi, T. Y. Seong and S. J. Park, *Phys. Rev. Lett.*, 2001, **86**, 1355–7.

45 B. Rezgui, A. Sabai, T. Nychyporuk, M. Lemiti, G. Bremond, D. Maestre and O. Palais, *Appl. Phys. Lett.*, 2010, **96**, 183105.

46 V. L. Dalal, J. Graves and J. Leib, *Appl. Phys. Lett.*, 2004, **85**, 1413.

47 C. Z. Chen, S. H Qiu, C. Q. Liu, Y. D. Wu, P. Li, C. Y. Yu and X. Y. Lin, *J. Phys. D: Appl. Phys.*, 2008, **41**, 195413.

48 U. Coscia, G. Ambrosone, S. Lettieri, P. Maddalena, V. Rigato, S. Restello, E. Bobeico and M. Tucci, *Sol. Energy Mater. Sol. Cells*, 2005, **87**, 433.

49 D. B. Beach and J. M. Jasinski, *J. Phys. Chem.*, 1990, **94**, 3019.

50 D. Das and M. Jana, *Sol. Energy Mater. Sol. Cells*, 2004, **81**, 169.

51 A. Matsuda, *J. Non-Cryst. Solids*, 1983, **59-60**, 767.

52 D. Das, *Solid State Phenom*,. 1995, **44-46**, 227.

53 A. S. Barnard, *Nanoscale*, 2009, **1**, 89.

54 M. Xu, S. Y. Huang, J. W. Chai, V. M. Ng, J. D. Long and P. Yang, *Phys. E*, 2006, **35**, 81.